

Evaluation of the Role of the Immune System Response After Minibeam Radiation Therapy

Annaig Bertho, Lorea Iturri, Elise Brisebard, Marjorie Juchaux, Cristèle Gilbert, Ramon Ortiz, Catherine Sebrie, Laurene Jourdain, Charlotte Lamirault, Gabriel Ramasamy, et al.

▶ **To cite this version:**

Annaig Bertho, Lorea Iturri, Elise Brisebard, Marjorie Juchaux, Cristèle Gilbert, et al.. Evaluation of the Role of the Immune System Response After Minibeam Radiation Therapy. International Journal of Radiation Oncology, Biology, Physics, In press, 10.1016/j.ijrobp.2022.08.011 . hal-03827260

HAL Id: hal-03827260
https://hal.science/hal-03827260

Submitted on 26 Oct 2022

HAL is a multi-disciplinary open access archive for the deposit and dissemination of scientific research documents, whether they are published or not. The documents may come from teaching and research institutions in France or abroad, or from public or private research centers.

L'archive ouverte pluridisciplinaire **HAL**, est destinée au dépôt et à la diffusion de documents scientifiques de niveau recherche, publiés ou non, émanant des établissements d'enseignement et de recherche français ou étrangers, des laboratoires publics ou privés.

INTERNATIONAL JOURNAL OF
RADIATION ONCOLOGY • BIOLOGY • PHYSICS
www.redjournal.org

BIOLOGY CONTRIBUTION

Evaluation of the Role of the Immune System Response After Minibeam Radiation Therapy

Annaig Bertho, PhD,[*,†,1] Lorea Iturri, PhD,[*,†,1] Elise Brisebard, MSc,[‡] Marjorie Juchaux, PhD,[*,†] Cristèle Gilbert, MSc,[*,†] Ramon Ortiz, MSc,[*,†] Catherine Sebrie, PhD,[§] Laurene Jourdain, MSc,[§] Charlotte Lamirault, PhD,[‖] Gabriel Ramasamy, MSc,[‖] Frédéric Pouzoulet, PhD,[‖,¶] and Yolanda Prezado, PhD[*,†]

[*]*CNRS UMR3347, Inserm U1021, Signalisation Radiobiologie et Cancer, Institut Curie, Université PSL, Orsay, France;* [†]*CNRS UMR3347, Inserm U1021, Signalisation Radiobiologie et Cancer, Université Paris-Saclay, Orsay, France;* [‡]*UMR703 — PAnTher — APEX, Oniris, Nantes, France;* [§]*Service Hospitalier Frédéric Joliot, CEA, CNRS, Inserm, BIOMAPS Université Paris-Saclay, Orsay, France;* [‖]*Département de Recherche Translationnelle, CurieCoreTech-Experimental Radiotherapy (RadeXp), Institut Curie, PSL University, Paris, France; and* [¶]*Inserm U1288, Laboratoire de Recherche Translationnelle en Oncologie, Institut Curie, PSL University, Université Paris-Saclay, Orsay, France*

Received May 26, 2022; Accepted for publication Aug 5, 2022

Purpose: Minibeam radiation therapy (MBRT) is an innovative technique that uses a spatial dose modulation. The dose distribution consists of high doses (peaks) in the path of the minibeam and low doses (valleys). The underlying biological mechanism associated with MBRT efficacy remains currently unclear and thus we investigated the potential role of the immune system after treatment with MBRT.

Methods and Materials: Rats bearing an orthotopic glioblastoma cell line were treated with 1 fraction of high dose conventional radiation therapy (30 Gy) or 1 fraction of the same mean dose in MBRT. Both immunocompetent (F344) and immunodeficient (Nude) rats were analyzed in survival studies. Systemic and intratumoral immune cell population changes were studied with flow cytometry and immunohistochemistry (IHC) 2 and 7 days after the irradiation.

Results: The absence of response of Nude rats after MBRT suggested that T cells were key in the mode of action of MBRT. An inflammatory phenotype was observed in the blood 1 week after irradiation compared with conventional irradiation. Tumor immune cell analysis by flow cytometry showed a substantial infiltration of lymphocytes, specifically of CD8 T cells and B cells in both conventional and MBRT-treated animals. IHC revealed that MBRT induced a faster recruitment of CD8 and CD4 T cells. Animals that were cured by radiation therapy did not suffer tumor growth after reimplantation of tumoral cells, proving the long-term immunity response generated after a high dose of radiation.

Conclusions: Our findings show that MBRT can elicit a robust antitumor immune response in glioblastoma while avoiding the high toxicity of a high dose of conventional radiation therapy. © 2022 The Author(s). Published by Elsevier Inc. This is an open access article under the CC BY-NC-ND license (http://creativecommons.org/licenses/by-nc-nd/4.0/)

Corresponding author: Annaïg Bertho, PhD; E-mail: annaig.bertho@curie.fr

This project received funding from the European Research Council (ERC) under the European Union's Horizon 2020 research and innovation program (Grant Agreement No 817908) and was also partially funded by SIRIC 2018 to 2022 (INCa-DGOS-Inserm_12554) and by France Life Imaging, grant ANR-11-INBS-0006. Calculation time was granted at the supercomputer Joliot Curie SKL (Irene_skylake) Très Grand Center de Calcul (TGCC) of Commissariat Energie Atomique (CEA), from the Partnership for Advanced Computing in Europe (PRACE Project Access Call 23rd, proposal number 2021240006).

Disclosures: none.

Research data are stored in an institutional repository and will be shared upon request to the corresponding author.

Supplementary material associated with this article can be found in the online version at doi:10.1016/j.ijrobp.2022.08.011.

Acknowledgments—The authors warmly thank Murielle Andrieu (CYBIO Core Facility, Institut Cochin, Université Paris Cité, CNRS, INSERM, F-75014 Paris, France) for cytokines dosage and Pays de la Loire, IBiSA, NeurATRIS, and Biogenouest for their support at the APEX platform, Nikon Center of Excellence at PAnTher INRAE/Oniris.

[1] Annaig Bertho and Lorea Iturri made equal contributions to this study.

0360-3016/$ - see front matter © 2022 The Author(s). Published by Elsevier Inc. This is an open access article under the CC BY-NC-ND license (http://creativecommons.org/licenses/by-nc-nd/4.0/)
https://doi.org/10.1016/j.ijrobp.2022.08.011

Introduction

Spatially fractionated radiation therapies (SFRT) rely on a compartmentalization of the radiation in smaller beam lines that allows for the radiation dose to be administered with less toxicity in the nontumoral tissue.[1] Radiation therapy treatments are highly restricted because of the surrounding normal tissue tolerances, especially in aggressive tumors located in sensitive tissues such as brain gliomas. Minibeam radiation therapy (MBRT)[2] is a type of preclinical SFRT that provides a high therapeutic index in difficult-to-treat cases, such as radioresistant tumors.[3-8] MBRT uses a strong spatial modulation of the dose, as the irradiation is performed with arrays of narrow parallel beams (0.5-1 mm) spaced 1.5 to 4 mm apart,[9] resulting in a highly heterogeneous dose distribution. The irradiated regions alternate in regions receiving very high doses (peaks) and low doses (valleys) (Fig. 1).[9]

The preclinical studies to date have shown that MBRT offers remarkable normal tissue sparing,[2-4,7,10-12] even at average doses of 20 Gy in 1 fraction.[6,13] Additionally, the tissue sparing demonstrated by MBRT might enable safe and effective use of hypofractionation schemes instead of 1.8 to 2 Gy per fraction over several weeks, which provokes the blood lymphopenia commonly seen in irradiated patients.[14] In contrast to other spatially fractionated techniques, such as microbeam radiation therapy (MRT)[15] or GRID,[16] the vast majority of studies on MBRT showed equivalent or superior tumor control compared with conventional seamless irradiation.[5,8,17-19]

In general, SFRT challenge the paradigm of conventional radiation therapy that lethal doses must be deposited in each of the tumoral cells to eliminate the tumor and suggest that other distinct biological mechanisms are activated. However, the underlying biological mechanisms in SFRT, including MBRT, remain elusive. Radiobiological experiments performed in SFRT, mainly using MRT, suggest a mixed contribution of radiation-induced bystander and abscopal effects,[20-24] vascular alterations,[25,26] and immunologic interactions.[15,27] However, a complete understanding of these processes is lacking.

In this study, we hypothesized that the high dose offered by MBRT might effectively prime the immune system. Although it has been long known that tumor responses to radiation therapy are hampered in the absence of T cells,[28] the optimal dose and temporal fractionation schemes to provoke an antitumoral immune response are still a subject of discussion.[29-31]

In the present study, we aimed to investigate the role of the immune system after MBRT in an in vivo rat model of glioblastoma, RG2, with a particular focus on T cells, but also other key players in radiation-induced immunity such as B cells and myeloid cells. To disentangle the specific effects of spatial fractionation from temporal fractionation or dose, 1 single fraction and the same mean dose were employed to compare conventional and MBRT irradiation modes. With the help of an immunodeficient rat model, anatomopathologic evaluation of the tissues, flow cytometry of the systemic and intratumoral immune cells, and multiparameter immunohistochemistry analysis of the tumors, we provided a first insight into the antitumoral immune response generated by MBRT. To our knowledge, this is the first evaluation of this kind in MBRT performed in an immunosuppressive syngeneic orthotopic rat model of glioblastoma.

Materials and Methods

All animal experiments were conducted in accordance with the animal welfare and ethical guidelines of our institution. They were approved by the French Ministry of Research (permit no 2019122418442057).

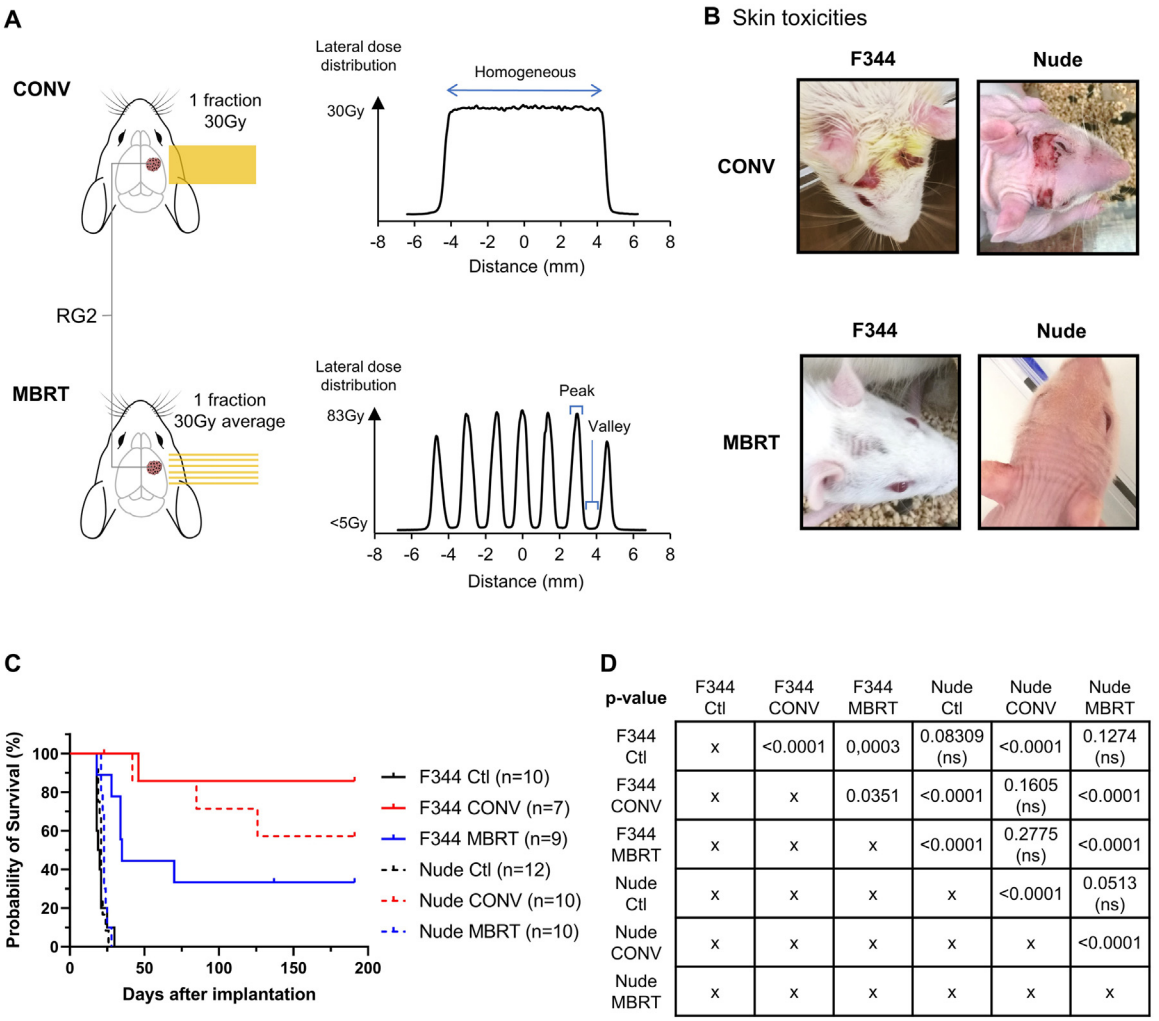
Tumor Inoculation

The RG2-[D74] (ATCC CRL-2433, RRID: CVCL_3581) glioma cell line, transfected with the luciferase gene, was used. RG2-Luc cells (5000) were suspended in 5 μL of DMEM and then injected intracranially into 6-week-old male immunocompetent rats (Fischer 344, Janvier Labs) or athymic rats (Nude, Janvier Labs) using a Hamilton syringe through a burr hole in the right caudate nucleus (coordinates relatives to Bregma: AP: −2.5 mm; ML: +4.7 mm; DV: 5.5 mm from the skull). Bioluminescence imaging (BLI) was done using an IVIS spectrum (PerkinElmer, Houten, the Netherlands) to confirm the presence of a tumor before irradiation, as described in previous works.[18]

In addition, 15 Fischer F344 rats were included in a "rechallenging" experiment, in which 7 naïve control animals and 8 experimental animals, which were previously inoculated with RG2 cells, received either MBRT (n = 4) or conventional irradiations (n = 4) after which the tumor was sterilized (verified by means of BLI and magnetic resonance imaging [MRI]). The animals were reinoculated with 5000 RG2-Luc cells in the left caudate nucleus 3 to 6 months after the first implantation.

Irradiation and dosimetry

Unilateral x-ray MBRT and conventional irradiation were applied using a small animal irradiator, as described previously.[5] As the goal of this study was to investigate which mechanisms are involved in tumor control, a dose of 30 Gy to the tumor was chosen. Radiation doses of at least 25 Gy are required to attain some tumor control in glioma-bearing rats after conventional irradiation[18,32] and, in particular, in this model (Fig. E1). However, conventional irradiation at these doses leads to extensive radiation-induced brain damage, but the animals survive long term and can be included in this study.[6] This level of dose would not be attainable in a human treatment with conventional therapy. In MBRT, a mean dose of 30 Gy was delivered to the tumor position, with peak and valley doses of 83 Gy and 4.5 Gy, respectively.



D

p-value	F344 Ctl	F344 CONV	F344 MBRT	Nude Ctl	Nude CONV	Nude MBRT
F344 Ctl	x	<0.0001	0,0003	0.08309 (ns)	<0.0001	0.1274 (ns)
F344 CONV	x	x	0.0351	<0.0001	0.1605 (ns)	<0.0001
F344 MBRT	x	x	x	<0.0001	0.2775 (ns)	<0.0001
Nude Ctl	x	x	x	x	<0.0001	0.0513 (ns)
Nude CONV	x	x	x	x	x	<0.0001
Nude MBRT	x	x	x	x	x	x

Fig. 1. (A) Graphical representation of the radiation plan used in this study. Rats were irradiated with one fraction of conventional photon radiotherapy (CONV) at the minimum dose for tumor control or with one equivalent fraction of mini-beam radiotherapy (MBRT). (B) Radiation-induced skin toxicities in immunocompetent F344 rats and immunodeficient Nude rats. CONV-irradiated rats developed radiation dermatitis while MBRT-irradiated rats only developed alopecia in the paths of the peaks. (C) Survival curves of F344 (solid line) or Nude (dashed lines) rat groups after CONV treatment (red), MBRT treatment (blue) or non-irradiated controls (black). (D) Pairwise comparison of the survival curves in panel C using Log-rank (Mantel-Cox) test. Head and brain silhouette sourced from: doi.org/10.5281/zenodo.3925903 and adapted. (For interpretation of the references to colour in this figure legend, the reader is referred to the web version of this article.)

The mean dose in MBRT is defined as the average dose between the first and last peaks of the lateral dose profile. At the tumor position, the beam width was 700 ± 40 μm, and the center-to-center (c-t-c) distance between minibeams was 1400 ± 100 μm. The irradiation was done 8 and 14 days after tumor inoculation for the survival studies and for the experiments involving immune phenotyping. Before the irradiation, 1 of the series (IHC) went through MRI to assess tumor volume. Tumor volume was 50.6 mm^3 on average, with an axial dimension of 4.4 mm. The axial dimension is orthogonal to the minibeam direction, so the tumor was irritated with approximately 3 to 4 minibeams (Fig. E2 presents a graphical representation).

Radiochromic films were then placed on the skin for quality assurance of the irradiation. Six groups of animals were evaluated.

Animal follow-up

The clinical status of the animals was evaluated 5 times per week. MRI acquisitions were performed for some rats using a 7-Tesla preclinical magnet (Bruker Advance Horizontal 7-T Bruker, Inc, Billerica, MA) and the same sequences as described in previous studies.[6]

MRI follow-up was performed at the following times: (1) 3 or 6 months after irradiation for long-term survival; (2) just before and at 12 and 25 days after the second injection of RG2 glioma cells for the "rechallenging" experiment. Any rat showing classical adverse neurologic signs associated with tumor growth was humanely euthanized (CO_2 asphyxia). During rat necropsy, the brains were removed and fixed in 10% neutral-buffered formalin for histopathologic and multiplex immunofluorescence (IF) analyses.

Analysis of peripheral and tumor immune cell populations by flow cytometry

Blood was collected in EDTA tubes. Red blood cells were lysed using a Red Blood Cell Lysis Solution (Miltenyi Biotec, Bergisch Gladbach, Germany). Tumors were dissected, and the tissues were incubated in digestion solution (DPBS containing 1 mg/mL Collagenase D [Roche], 0.1 mg/mL DNase I [Sigma], and 3% fetal calf serum [FCS]). Tissues were then mechanically disrupted to obtain a single-cell suspension in flow cytometry staining (FACS) buffer (DPBS with 0.5% bovine serum albumin [BSA] and 2 mM EDTA). Cells were mixed with 30% isotonic Percoll Solution, centrifuged, and blocked with anti-CD32 (FcγRII) blocking agent.

Cells were treated with a viability stain diluted 1:1000 (FVS780, BD Biosciences, RRID: AB_2869673) and immunolabeled in buffer containing PBS and 3% of fetal bovine serum (Table E1). Counting beads were added to the sample before acquisition (CountBright Plus Absolute Counting Beads, Thermo Fisher). Cell profiles were analyzed using a flow cytometer (Fortessa LSR, BD Bioscience) and FlowJo v10.6.

Analysis of systemic cytokines

After collection in a heparin tube, the whole blood was centrifuged at 4°C at 1500 g for 15 minutes and plasma was separated. Six cytokines (IL-1β, IL-6, IL-10, KC/GRO [CXCL1] TNFα, and IFNγ) were measured using chemiluminescence-based V-PLEX Proinflammatory Panel 2 Rat Kit (MSD, K15059D, RRID: AB_2916285).

Histopathology

The brains were trimmed in several coronal sections and embedded in paraffin. Serial 4-μm-thick sections were cut, and 1 slide was stained with hematoxylin and eosin (HE) for histopathologic evaluation, whereas other slides were used for IHC. All histopathologic assessments were performed blinded by a European College of Veterinary Pathologists diplomate pathologist.

Multiplex immunofluorescence staining

Multiplex IF staining was done to identify the major subpopulations of T cells and macrophages using a panel of 5 antibodies (CD3 [1:600, A0452, Dako, RRID: AB_2335677], CD4 [1:200, 25229, Cell signalling, RRID: AB_2798898], CD8 [OX-8, 1:400, ab33786, Abcam, RRID: AB_726709], FoxP3 [EPR2210237, 1:100, ab215206, Abcam, RRID: AB_2860568] and CD68 [ED1, 1:200, MCA341R, BioRad, RRID: AB_2291300]) and an Opal Multiplex IHC (Akoya Bioscience), which was optimized in house. Successive cycles were done by incubating with each primary antibody diluted in normal goat serum 5% (S2000-100, Dutscher). The slides were then incubated with secondary antibody at a 1:300 dilution (Goat antirabbit P0448, Dako, RRID: AB_2617138 or goat antimouse P0447, Dako, RRID: AB_2617137) followed by incubation with Opal fluorochrome diluted at 1:100 in Plus Amplification Diluent (FP1498, Akoya Biosciences). These cycles were repeated for subsequent antibodies. Finally, the slides were stained with DAPI (D1306, Invitrogen, RRID: AB_2629482) at a 1:1000 dilution and mounted using an in-house preparation of Mowiol.

Image acquisition and analysis

The Mantra 1 quantitative pathology workstation (PerkinElmer) was used for image acquisition. The chromogenic IHC-stained slides were imaged with the brightfield protocol, and the multiplexed IF- stained slides were imaged with the fluorescence protocol (MantraSnap 1.0.4 software, Akoya Bioscience). Two sets of images were acquired per slide: 1 set with images centered on the edge of the tumor and 1 set of images acquired more centrally within the tumor. InForm advanced image analysis software (InForm 2.4.4 software, Perkin Elmer) was used to process and analyze the multispectral images (Fig. E3 shows an example of acquired images).

Statistical analysis

The log-rank (Mantel-Cox) test was used to analyze the survival data. For the analysis of FACS's data, the results are presented as the means $\pm$ standard error of the mean. Statistical analyses were performed using a Brown Forsythe and Welch analysis of variance with multiple comparisons using the unpaired t test for the peripheral immune cells. Statistical analyses were performed using 1-way analysis of variance with multiple comparison using uncorrected Fischer's LSD test for the intratumoral immune cell infiltration and circulating cytokines.

A linear mixed model with repeated measures using the restricted maximum likelihood method for (co)variance component estimation procedure was employed for the statistical analysis of IHC quantitative data because the data were not independent (numerous data per animal, ie, 1 per analyzed image).

All statistical analyses were performed using GraphPad Prism 9 software (GraphPad Software, CA), except for the data from the histopathologic analyses, which were analyzed using R software version 4.0.4 (R Core Team, 2021).

Results

Survival curves and clinical symptoms of glioblastoma-bearing immunocompetent and immunodeficient rats

Figure 1 presents a schema of the irradiation configurations. Figure 1 also shows some radiation-induced skin toxicities

observed and the survival curves for the different groups along statistical analysis.

None of the immunocompetent animals receiving MBRT developed any skin toxicity, whereas 2 out of 10 of the nude rats in group 5 exhibited a light skin injury (Fig. 1B). A transient radiation-induced alopecia appeared 6 to 7 days after MBRT on the path of the minibeams. In contrast, all animals receiving conventional irradiation developed severe radiation-induced dermatitis. Immunodeficient rats exhibited moist desquamation 8 to 10 days after irradiation. Immunocompetent rats developed the same type and grade of lesion with a later onset (14-18 days after irradiation, Fig. 1B).

No significant dependence on the immune status of the animals was observed in the survival curves after conventional irradiation; however, the number of long-term surviving animals free of tumors was higher in the immunocompetent group (89 %) compared with the immunodeficient group (62.5 %) (Fig. 1C). MBRT-irradiated immunodeficient rats did not respond to the treatment, in contrast to the immunocompetent rats. A significant percentage (33%) of the MBRT-treated immunocompetent animals survived long-term despite about half of the tumor volume receiving a dose lower than the prescribed one because the irradiation in MBRT is done with 700 μm peaks spaced by 700 μm (see Fig. 1A and E2). This nonresponse to MBRT in athymic rats, lacking mature T cells, suggests a key role for T cells in the mechanism of tumor elimination by MBRT. These results indicate that different mechanisms are responsible for the effects of the 2 different types of irradiations. Tumor presence was confirmed in all animals sacrificed in the first 3 months after irradiation.

A

	Histopathological findings related to tumor growth and elimination		Radiation-induced histopathological injuries	
	CONV-RT	MBRT	CONV-RT [1]	MBRT
Long-term	Cavitation (9/9) Ventriculomegaly (9/9) Glial scars (9/9) Gliosis (9/9)	Cavitation (4/4) Ventriculomegaly (4/4) Glial scars (4/4) Gliosis (4/4) Hemosiderin-laden macrophages/ microglia (4/4) Lymphocytic perivascular cuff (3/4)	Necrosis (ventricle, plexus choroid) (9/9) Edema (3/9) Thickened blood vessel (4/9) Vascular thrombosis and necrosis (4/9) Marked mineralization (6/9) Leukocytoclastic vasculitis (3/9) Hippocampal and fornix neuronal degeneration (9/9) Increased of Iba1 staining (microglia) in the striatum, thalamus and pons (9/9)	Minimal to mild foci of mineralization in the thalamus and corpus striatum (4/4)

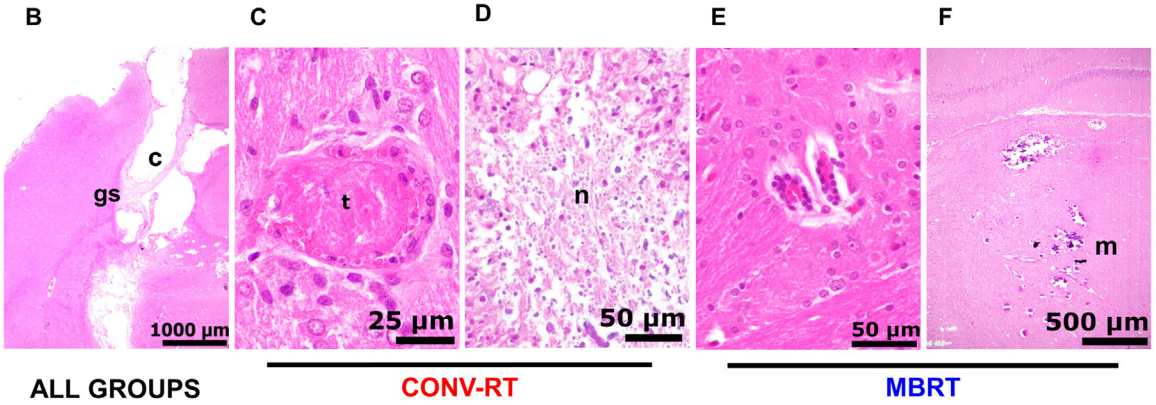


Fig. 2. (A) Table summarizes histopathological changes observed in immunocompetent and immunodeficient rats, related to tumor growth and elimination and radiation-induced injuries, at 6 months' post-irradiation (long-term survivors from the survival group). (B) Cavitation and glial scar are observed at low magnification, in place of the tumor, observed in all groups and due to tumor inoculation and elimination. (C) Vascular thrombosis observed in the CONV-RT group, t: thrombosis. (D) Necrosis observed in the CONV-RT group, n: necrosis. (E) lymphocytic perivascular cuffing observed in the MBRT group. (F) Foci of mineralization observed in the MBRT group (m: mineralization). [1] radiation-induced late injuries are independent from the immune status of the rat.

Histopathologic and MRI findings

The histopathology analysis at 7 days after irradiation revealed differences in the tumor cell morphology between groups. In the nonirradiated group, the cells displayed a spindle-shaped morphology corresponding to the usual microscopic appearance of RG2 glioma.[33] In the conventionally irradiated group, tumors were predominantly composed of neoplastic giant cells with marked nuclear atypia. This change in tumor cell morphology was consistent with irradiation-induced cell cycle alterations. In the animals receiving MBRT, the tumors presented a mixed pattern intermediate between nonirradiated and conventionally irradiated tumors, which was likely the result of the heterogeneous dose distribution.

Six months after conventional irradiation, the histopathologic analysis reported severe radiation-induced brain injuries in all long-term surviving rats from conventional groups, which was independent of their immune status (Fig. 2). Radiation-induced brain injuries were composed of necrosis (around the ventricle and in the plexus choroid), edema, vasculopathy, marked mineralization, hippocampal and fornix neuronal degeneration, and increased microglia, seen by IBA-1 staining. Other findings were associated with tumor growth and elimination. Accordingly, MRI images exposed blood-brain barrier breakdown (BBB) in the hippocampus and subiculum (4/5 immunodeficient rats, 4/6 immunocompetent rats), localization of which matched the injuries detected in the histopathologic analysis (Fig. E4).

In contrast, there was a remarkable reduction in radiation-induced brain damages in the MBRT-irradiated group consisting of localized and micrometric foci of mineralization located in the thalamus and less evident in the corpus striatum (Fig. 2). Other histopathologic findings in the MBRT-irradiated group were mainly related to tumor growth and elimination, in agreement with the MRI images (Fig. 2 and E4). Among the MBRT-irradiated animals, only a few animals (n = 4) were imaged between 3 and 6 months after irradiation, and no radiation-induced brain injuries were observed (Fig. E4).

Analysis of peripheral immune cell populations and systemic cytokines

Because of the observations of inflammatory processes and the possibility of a radiation-induced lymphopenia due to brain irradiation,[34] we analyzed blood leukocytes and cytokines in search of radiation-induced changes in the systemic immune environment.

The circulating peripheral immune cells were quantified in the blood 24 hours and 7 days after irradiation (Fig. 3A-G). 24 hours after irradiation, and no significant changes in any of the evaluated population types were observed except for CD4 T cells, whose numbers increased in the MBRT group. A slight decrease in CD4 T cells was also observed 7 days postirradiation with MBRT. A decrease in the CD8 T cells was also observed at 7 days after irradiation in both the MBRT and conventional groups, compared with the nonirradiated group, with no difference between irradiated groups. Conventional irradiation reduced the number of circulating NK cells compared with controls and B cells at 7 days postirradiation compared with the MBRT group. Neutrophil proportions in the blood tended to be increased by MBRT compared with conventional irradiation at 7 days after irradiation, but without any difference compared with the nonirradiated controls. This suggests a slight inflammation triggered by MBRT.

$CD43^{low}$ $His48^{high}$ monocytes decreased similarly at 24 hours after conventional and MBRT irradiations compared with the control group. At 7 days after irradiation, $CD43^{low}$ $His48^{high}$ population reach basal level in the MBRT group, whereas the population was still decreasing in the conventional group. MBRT increased the proportion of $CD43^{high}$ and $His48^{low}$ at 7 days after irradiation exposure compared with the nonirradiated controls. There was a tendency for this population to be increased compared with conventional irradiation, although the difference was deemed insignificant. Overall, MBRT tends to create an inflammatory phenotype 7 days after irradiation compared with conventional irradiation. The details of the gating strategy are available in Figure E5.

Inflammatory cytokines released after irradiation can support and modulate the immune response. Radiations seemed not to significantly affect plasmatic IL1-β levels, although some samples were below the detection threshold. IL-6 and IL-10 exhibited a fast increase 24 hours postirradiation in the MBRT group, whereas they increased at 7 days postirradiation in the conventional radiation therapy group. Accordingly with the MBRT-induced increase of neutrophils in the blood flow at 7 days postirradiation, MBRT-irradiated animals exhibited an increase in the release of KC/GRO (CXCL1). On the contrary, MBRT tended to decrease the levels of plasmatic TNF-α and IFN-γ compared with conventional radiation therapy at 7 days postirradiation, after a slight early increase (Fig. 3H-M).

Immune cell infiltration

Intratumoral immune cell infiltration measured by flow cytometry

Flow cytometry was performed 7 days after irradiation. A significant alteration in the immune cell composition of the tumors was evident, specifically T cells (Fig. 4A). T cells (characterized as $CD3^+$ cells) represented 19% of the hematopoietic cells in the control group, 47% in the conventional radiation therapy group, and 42% in the MBRT group, with no significant difference between the 2 irradiated groups. Interestingly there was an increase in the proportion of regulatory T cells (Tregs, characterized as $CD4^+$ $CD25^+$ T cells) with respect to the remainder of the $CD4^+$ conventional T cells in the irradiated groups (see Fig. 4B, D), with no significant difference among them. No differences were observed in the proportion of tissue-resident memory T cells (TRM, characterized as $CD8^+$ $CD103^+$ T cells)

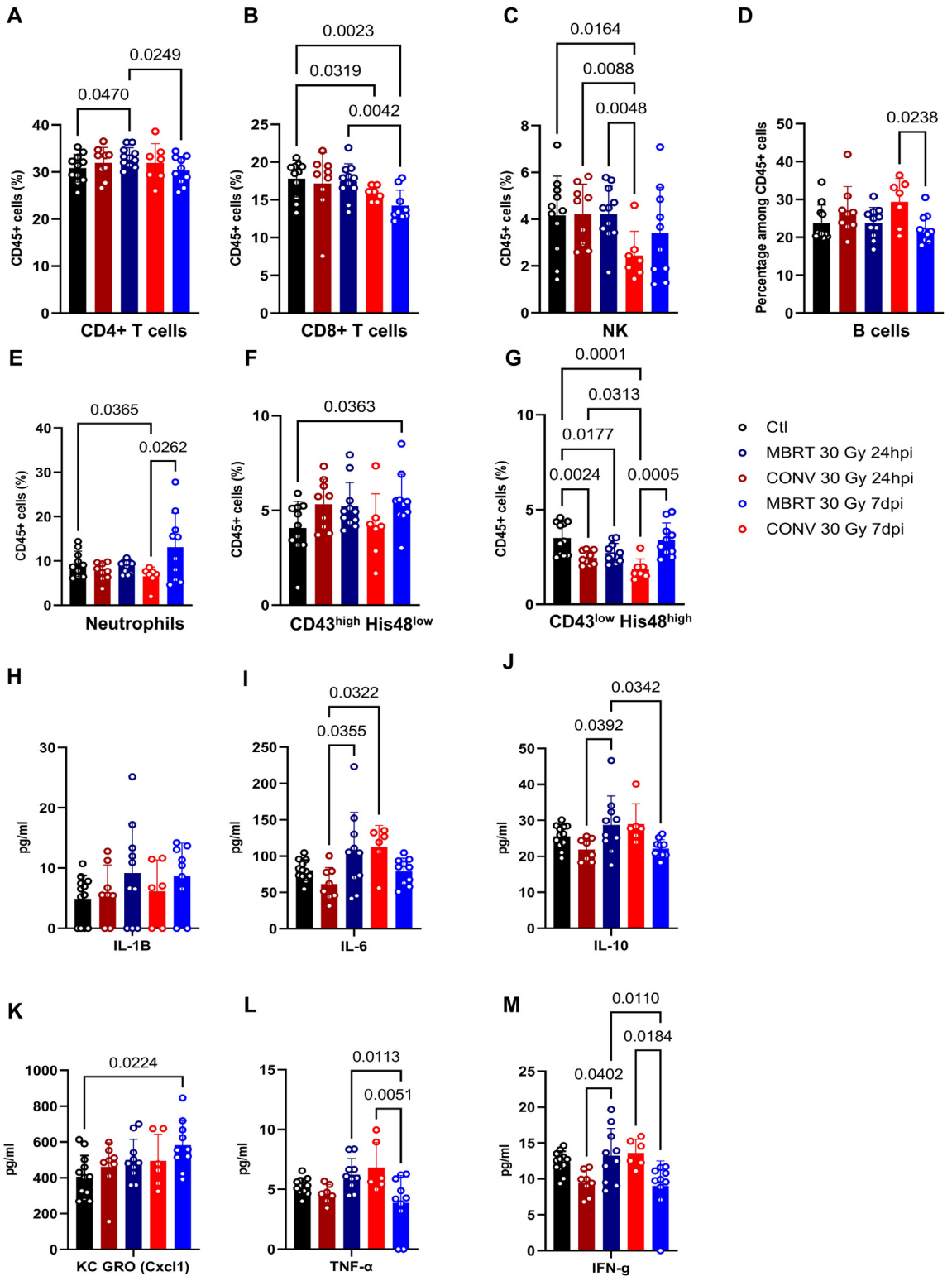


Fig. 3. Impact of irradiation type on the circulating immune cell population and cytokines. (A) CD4+ T cells; (B) CD8+ T cells; (C) NK; (D) B cells; (E) Neutrophils; (F) CD43^{high} His48^{low} monocytes; (G) CD43^{low} His48^{high} monocytes. Gating strategy is presented in supplemental materials, figure S4. Concentrations of circulating cytokines in the blood for (H) IL1β (I) IL-6 (J) IL-10 (K) KC/GRO (CXCL1) (L) TNF-α and (M) IFN-γ.

with respect to the remainder of the cytotoxic $CD8^+$ T cells (Fig. 4C). The details of the gating strategy are available in Figure E6.

Overall, there were 11- and 13-fold average increases in T-cell density in the tissue of the conventional and MBRT groups, respectively. This infiltration was found in all T-cell subpopulations analyzed, including $CD4^+$ and $CD8^+$ T cells, and for Tregs and TRM T cells. Among the T-cell population, $CD8^+$ T cells were present at a higher abundance in the tissue (Fig. 4B-F). This suggests the establishment of an adaptive immune response in situ as suggested by the survival curves.

Moreover, a significantly higher immune cell density was also observed for other key players in the immune response in the irradiated groups with respect to the controls, notably for B cells, a population that is practically nonexistent in nonirradiated tumors, which were 40- and 52-fold higher in conventional and MBRT, respectively (Fig. 4G). MBRT-treated rats exhibited a significantly higher density of NK cells, which was slightly higher compared with that for conventional radiation therapy (Fig. 4). Although the differences among the irradiated groups were deemed not significant, there was a trend toward a higher cell density of these populations in the MBRT group.

Intratumoral immune cell infiltration measured by immunochemistry

Multiplexed IHC staining was performed to identify differences in the spatial distribution and kinetics of immune infiltration among groups. Two areas of interest were evaluated: the center and the periphery of the tumor tissue (Fig. 5).

Two days after irradiation, MBRT-irradiated rats exhibited a significantly higher T cell infiltration in the center of the tumor compared with the conventionally irradiated animals. This was the case for $CD8^+$ cytotoxic T cells ($CD3^+$ $CD8^+$ $CD4^{neg}$), $CD4^+$ T helpers ($CD3^+$ $CD8^{neg}$ $CD4^+$), as well as double positive (DP, $CD3^+$ $CD8^+$ $CD4^+$) (Fig. 5). No differences in Tregs ($CD3^+$ $CD4^+$ $FOXP3^+$) and double negative T cells ($CD3^+$ $CD4^{neg}$ $CD8^{neg}$) among the groups were observed (Fig. E6). The latter 2 cell types were not abundant. In contrast, $CD8^+$ and DP T cells were the most abundant types in the center of the tumor in the MBRT-irradiated group. In the periphery, MBRT-irradiated rats exhibited a significantly higher infiltration of $CD4^+$ helper T cells and DP, but not $CD8^+$ cytotoxic T cells (Fig. 5).

Seven days after irradiation, the T-cell infiltration increased in both the conventional radiation therapy and MBRT groups (Fig. E7). In the center of the tumor, a higher T-cell infiltration was observed in the conventionally irradiated group, with significantly higher $CD4^+$ T helper and DP T-cell densities compared with the other groups, but not Treg or $CD8^+$ T cells. MBRT-irradiated rats showed a higher density of $CD8^+$ cytotoxic cells and $FoxP3^+$ Tregs in the periphery of the tumor. Taken together, significant differences were observed with respect to the spatial distribution of T cells at different time points of the analysis. The results suggest that MBRT provokes a faster infiltration of T cells in the center of the tumor, specifically $CD4^+$, $CD8^+$, and DP lymphocytes, whereas 7 days postirradiation, the significant infiltration of T cells is concentrated in the tumor periphery, which contrasted with that observed for the conventional radiation therapy group. Conventionally irradiated tumors exhibited a higher infiltration at macrophages in the periphery of the tumor 7 days postirradiation. Interestingly, conventionally irradiated tumors' centers had also a significantly higher concentration of CD8+ macrophages compared with MBRT-irradiated tumors and controls at both time points.

Figure E8 shows the dynamic of tumor infiltration by immune cells between 2- and 7-days postirradiation. A significant increase in infiltration was observed at day 7 compared with day 2. It should also be noted that T-cell infiltration in tumor center was diffuse in both the conventional radiation therapy and MBRT-irradiated groups. However, T cells tended to cluster around vessels in the MBRT-irradiated groups (Fig. E9).

Long-term antitumor immunity

To explore the potential long-term antitumor immunity triggered by MBRT, cured rats from the MBRT or conventional survival group (ie, long term-survivors) were rechallenged with a second injection of RG2 cells. Figure E10A represents the experimental design. All the naïve controls were found to have developed tumors and were euthanized because of clinical signs in the expected period. The tumor presence was verified by bioluminescence (Table E2) and MRI before sacrifice (Fig. E10B).

None of the previously irradiated animals (MBRT n = 4, conventional n = 4) developed a macroscopic tumor, as determined by bioluminescence (7, 14 and 30 days after reinjection) and MRI (12 and 25 days after reinjection). As expected, rats from group 3 (conventional radiation therapy) exhibited severe radiation-induced brain damage 6 months postirradiation, whereas group 5 (MBRT) did not.

Discussion

MBRT is an innovative radiation technique that relies on the spatial fractionation of the dose and provides a high therapeutic index in radioresistant tumors.[3-8] The spatial configuration of the irradiation allows for certain regions to be targeted with high doses (peaks) and low doses (valleys) of radiation. Several reports have shown that RT can lead to immune activation or immunosuppression, depending on the radiation scheme—including dose, fractionation, and overall treatment time—but also tumor type and location.[29-31] The optimal radiation scheme to elicit an effective antitumoral response is still unknown.[35-37] RG2 is a very invasive and low immunogenic syngeneic rat glioblastoma model,[33] similar in this sense to human glioblastomas, where the microenvironment is highly immunosuppressive and tumor-associated macrophages (TAM) constitute the

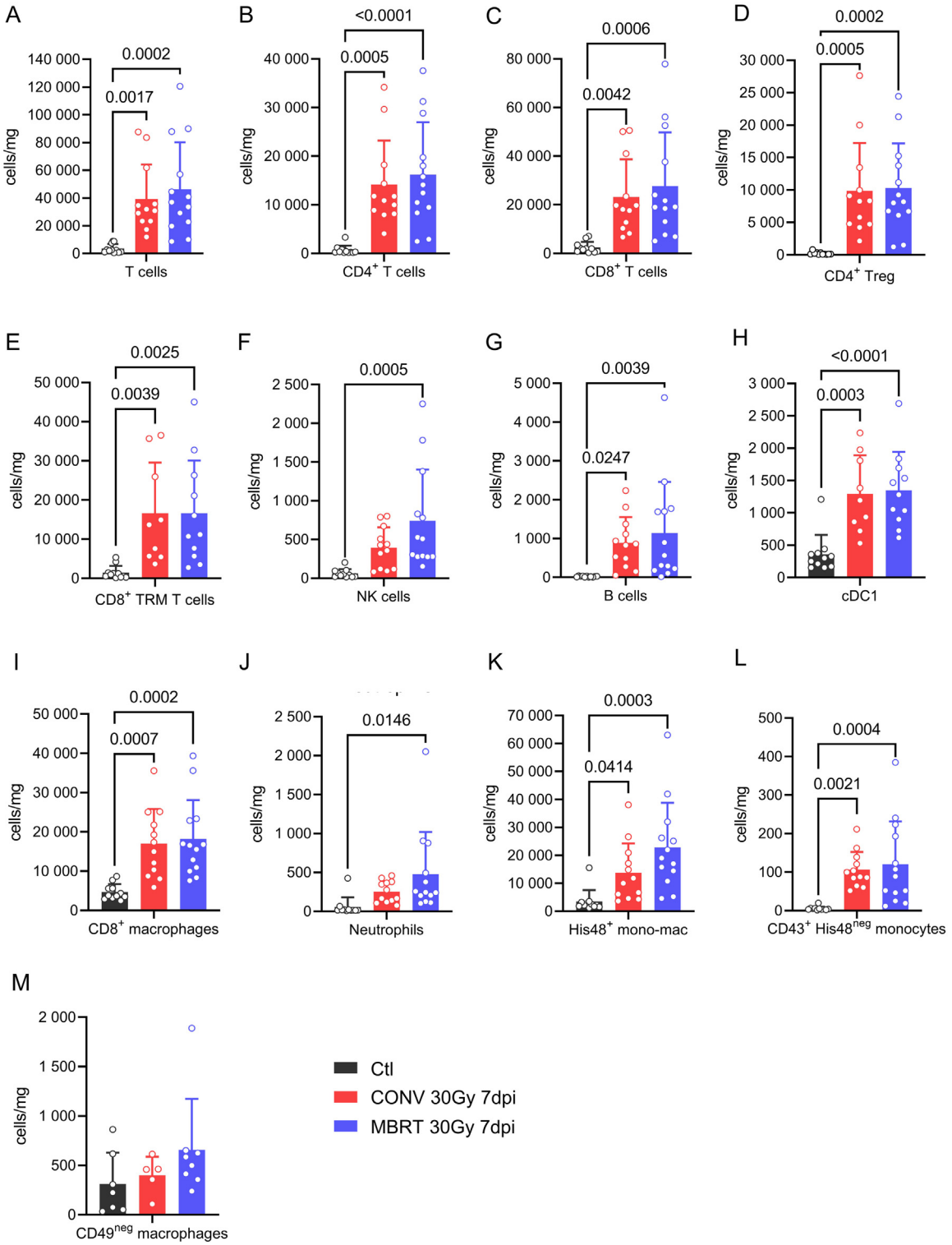


Fig. 4. Flow cytometry analysis of immune cells in glioblastoma. (A) T cells, (B) CD4+ T cells, (C) CD8+ T cells, (D) Tregs, (E) TRM T cells, (F) NK cells, (G) B cells, (H) cDC1, (I) CD8+ macrophages, (J) neutrophils, (K) His48+ monocytes-macrophages (mono-macs), (L) CD43+ His48neg monocytes and (M) CD49dneg macrophages. Control (n = 11), conventional radiotherapy (n = 12), and MBRT (n = 13).

majority of tumor immune cells.[38] We hypothesized that the high dose delivered in the peak regions of MBRT would be enough to elicit an inflammatory response that might activate an antitumoral immune response in this model. High doses in SFRT have been shown to create an antitumoral immune response in subcutaneous models.[16,39]

It is worth noting that the "conventional" radiation therapy-treated group in this study received a very high dose of

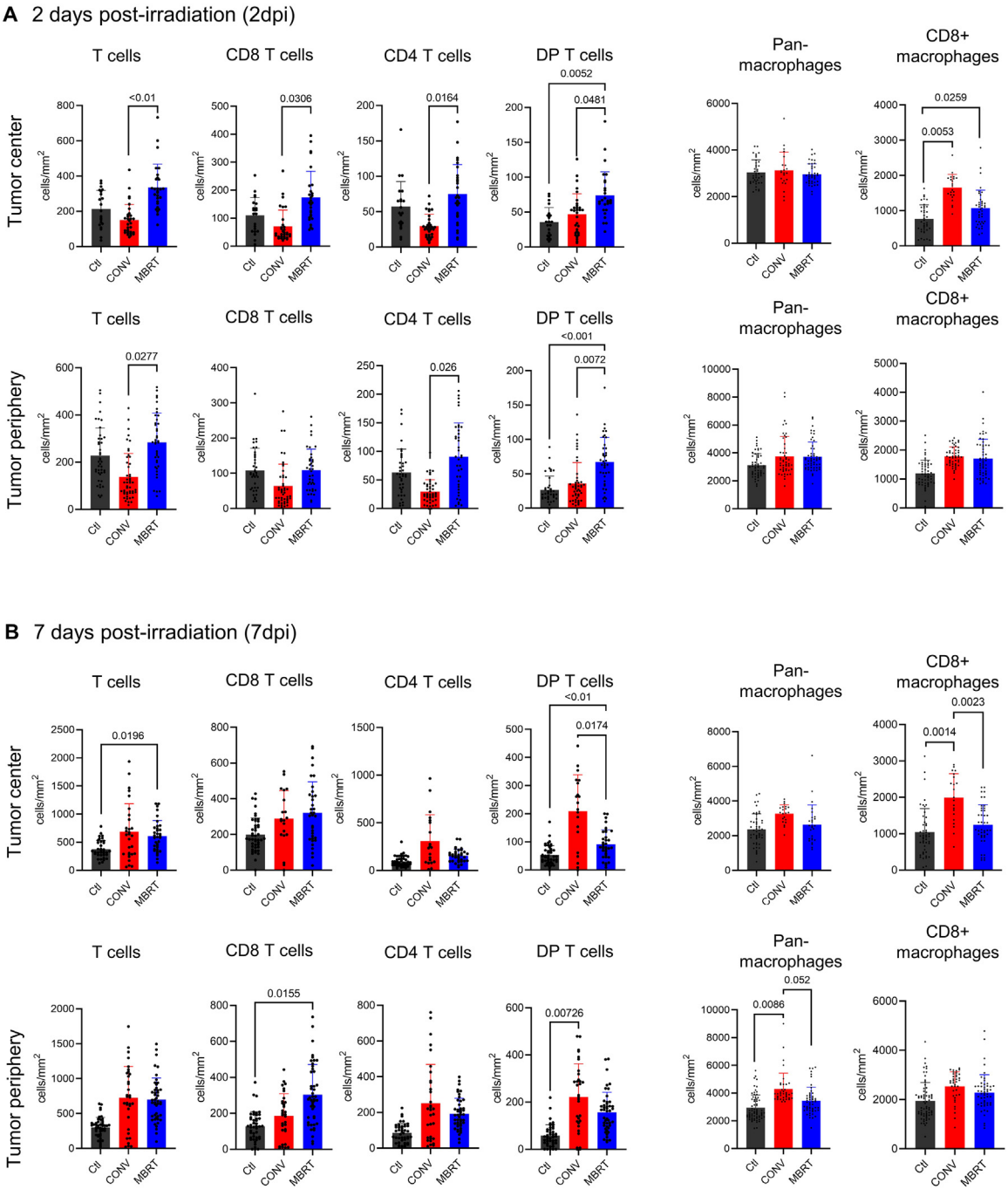


Fig. 5. T cell and macrophage densities (cells/mm^2) 2 days (A) and 7 days (B) after irradiation in the center or the periphery of the tumor. T cell subpopulations were classified in CD8+, CD4+, CD8+ CD4+ (DP). Pan-macrophages were detected as CD68+ cells, and coexpression with CD8 was observed. Subpopulation of CD4+ FoxP3+ regulatory T cells and CD4-CD8- (DN) T cells are presented in Figure S6.

radiation that is not attainable in human treatment. Most studies on spatially fractionated radiation therapy in synchrotrons compared SFRT to 1 fraction of conventional RT that differed between studies, although frequently similar to the valley dose (5-15 Gy), and which generally does not offer tumor control or incite a sufficient immune response when given in 1 fraction.[39-41] In our study, both groups had tumor control in at least 30% to 40% of the animals.

MBRT might influence peripheral immune cell populations differently compared with conventional irradiation through secretion of pro- and anti-inflammatory cytokines in the blood. Indeed, MBRT upregulated the secretion of IL10 (anti-inflammatory cytokine secreted by B-cells and macrophages), and proinflammatory cytokines such as IL-6 (pleiotropic effects on various immune cells, including T cells)[42-44] or IFN-γ (supporting T cells' infiltration in the tumor) which

is rapidly released after MBRT in coherence with our observations of a rapid T-cells intratumoral infiltration.[45,46] In contrast, the levels of plasmatic TNF-α, another proinflammatory cytokine linked to development of chronic inflammation and radiation-induced brain damage[47-49] are reduced in MBRT compared with seamless irradiations. KC/GRO (chemoattractant of neutrophils and myoloids cells) is also upregulated in MBRT compared with conventional radiation therapy.[50] Both radiation groups provoked a massive infiltration of different immune cell types in the stroma of the tumor, including effector and immune response regulators as CD4 and CD8 T cells. A significant increase of B cells and antigen presenting cDC1 dendritic cells and $CD8^+$ macrophages (by their expression of Rt1b/MHC-II) were indicative of an adaptive immune response. This was likely due to the release of neoantigens, immunogenic cell death signals, and proinflammatory cytokines released in the tumor microenvironment after radiation therapy, as has been shown previously in the literature.[36,37,51] Tumor infiltrating B cells have been shown to provide long-term immunity through antigen presentation to T cells and the production of tumor-specific antibodies.[52] Moreover, recent clinical studies indicate that B cells in tumors, especially co-occurrence with tumor-associated $CD8^+$ T cells, are associated with an improved survival[53] and are a significant predictor of response to immunotherapy.[53-55] The long-term antitumor immunity obtained by radiation therapy was demonstrated in both groups after rechallenging the system with the reimplantation of tumoral cells. Because the purpose of this study was to determine the immune response generated after MBRT, we did not phenotype the large heterogeneity existing among tumor infiltrating lymphocytes (TIL), which could have provided greater understanding in terms of function[56,57] and exhaustion phenotypes.[58]

Importantly, we observed pivotal differences in conventional radiation therapy and MBRT related to T cell dependence and kinetics of T cell infiltration. The lack of response in MBRT-treated athymic animals demonstrated that T cells have a key role in MBRT's mode of action, while dispensable in the case of conventional ablative RT, showing that MBRT offers tumor control by a fundamentally distinct manner. Additionally, significant T cell infiltration was observed as early as 48 hours after treatment, compared with controls and conventional radiation therapy, including in the center of the tumor. This might be indicative of a faster and more efficient T cell recruitment to the tumor microenvironment. Although immune cell killing after conventional radiation therapy could not be excluded at this time point, no significant difference was observed between the controls and conventional radiation therapy.

Additionally, we observed a significantly different organization of $CD8^+$ macrophages in the tumor, as only the conventionally irradiated group had a higher concentration of these cells in the center of the tumor. These results might be explained by specific cell signaling pathways activated in the tumor or bystander effects of SFRT. MRT studies in synchrotrons have shown that MRT leaves vascular walls intact but provokes apoptotic endothelial disruption in the paths of the beams, which can lead to lower oxygenation and tumor necrosis.[26,59] Endothelial disfunction increases the expression of adhesion molecules ICAM, VCAM, endothelial leukocyte adhesion molecule (ELAM/E-selectin), and integrins, and thus facilitates the recruitment and attachment of circulating leukocytes to the vessel wall.[60] Indeed, it was observed that T-cells tended to be found clustered around vessels mainly in the MBRT-irradiated animals. Another explanation might be physico-chemical: the levels of oxygen present in the tumor could be different after MBRT. Indeed, the percentage of necrotic areas in the tumor was larger in the MBRT-irradiated animals in comparison with those receiving conventional radiation therapy at 7-days postirradiation (Fig. E11). Seven days after MBRT the tumoral tissue is interspersed by large coalescing areas of necrosis. On the contrary, in the conventional radiation therapy group, the necrosis remained limited to small and multifocal foci. It is known that levels of hypoxia in the tumor can modulate cytotoxic T cell function.[61] Molecular signals released by epithelial or cancer cells might also be more immunostimulatory in the case of MBRT. T cell response is likely to be crucial for MBRT because it does not depose an ablative dose in each of the cells.

It should be also noted that in this study we did not directly evaluate the effect of the transfection of tumor cells with

Table 1 Details of groups included in the study

Group	IRRADIATION	TYPEOF ANIMAL	MEAN DOSE (TUMOR)Gy	PEAK DOSEGY	VALLEY DOSEGY	NO. OF ANIMALS		
						Survival	IHC	FACS
1	Nonirradiated	Immunocompetent	0	N/A	N/A	10	10	11
2	MBRT	Immunocompetent	30	83	4,5	9	10	13
3	Conventional	Immunocompetent	30	N/A	N/A	7	10	12
4	Nonirradiated	Immunodeficient	0	N/A	N/A	12	5	N/A
5	MBRT	Immunodeficient	30	83	4,5	10	5	N/A
6	Conventional	Immunodeficient	30	N/A	N/A	8	N/A	N/A

Abbreviations: FACS = flow cytometry; IHC = immunohistochemistry; MBRT = minibeam radiation therapy.

luciferase. The potential immunogenicity of luciferase may slow down in vivo tumor growth in some models,[62] although it has been seen not to have any effect on tumor response on some others, such as ovarian cancer.[63] The median survival time of the control RG2-Luc bearing rats in our studies (20 ± 2 days) is equal within the uncertainty bars to other works that used the wildtype RG2 cell line at similar concentrations,[64,65] suggesting that the effect of luciferase transfection might be not significant in our model.

Although the most effective dose and fractionation for immune priming has not been fully elucidated,[66,67] it is well established that radiation therapy in conventional fractionation schemes (2 Gy per fraction) is not usually effective in eliciting an immune response.[35] Hypofractionation schemes with high doses per fraction are more likely to trigger a favorable TME by inducing immunogenic cell death and subsequent immune cell infiltration.[68] However, the use of those fractionation schemes is restricted in large tumors by the tolerances of the surrounding normal tissues.

Our study shows that very high and immune-priming doses could be delivered with MBRT with reduced toxicity. This offers promise for effective combinations with immunotherapies. Although MBRT is still at a preclinical stage, our results may guide the design of clinical trials in some other SFRT techniques, such as GRID[69] and LATTICE therapy,[70] which also use high doses in hypofractionation schemes. Our results might be especially useful when designing trials combining SFRT and immunotherapy in terms of optimal drugs and timing. Although from our study we cannot conclude which is the most relevant dosimetric parameter in SFRT to activate the immune system, we can state that this is observed with very low valley doses (<5 Gy). Further studies on the influence on the different dosimetric parameters (peak and valley doses, PVDR) and temporal fractionation on the immune response of MBRT are warranted.

Conclusion

The present study provides a first insight into the antitumoral response generated by MBRT with a particular focus on T cells. One fraction of high-dose photon radiation initiated an efficient antitumoral response, and importantly, MBRT accomplished this response with minimal radiation-associated toxicities, as shown in this and previous studies.[2-4,6,8,10,12]

Many radiobiological mechanisms are emerging to explain the effectiveness of new radiation therapy techniques such SFRT, including MBRT, and their proper study is crucial for a rapid and efficient clinical transfer for ongoing or future clinical trials.

The strong immune response generated after a single nontoxic fraction of radiation therapy places MBRT as a promising candidate for future studies that focus on combinations with immunotherapies Table 1.

References

1. Prezado, Y., *Divide and conquer: spatially fractionated radiation therapy,* Expert reviews in molecular medicine, 2022. **in press**.
2. Dilmanian FA, Zhong Z, Bacarian T, et al. Interlaced x-ray microplanar beams: A radiosurgery approach with clinical potential. *Proc Natl Acad Sci U S A* 2006;103:9709-9714.
3. Prezado Y, Deman P, Varlet P, et al. *Tolerance to Dose Escalation in Minibeam Radiation Therapy Applied to Normal Rat Brain: Long-Term Clinical, Radiological and Histopathological Analysis. Radiat Res* 2015;184:314-321.
4. Deman P, Vautrin M, Edouard M, et al. Monochromatic minibeams radiotherapy: From healthy tissue-sparing effect studies toward first experimental glioma bearing rats therapy. *Int J Radiat Oncol Biol Phys* 2012;82:e693-e700.
5. Prezado Y, Sarun S, Gil S, Deman P, Bouchet A, Duc GL. *Increase of lifespan for glioma-bearing rats by using minibeam radiation therapy. J Synchrotron Radiat* 2012;19:60-65.
6. Prezado Y, Santos MD, Gonzalez W, et al. *Transfer of Minibeam Radiation Therapy into a cost-effective equipment for radiobiological studies: a proof of concept. Sci Rep* 2017;7. https://doi.org/10.1038/s41598-017-17543-3.
7. Prezado Y, Jouvion G, Hardy D, et al. *Proton minibeam radiation therapy spares normal rat brain: Long-Term Clinical, Radiological and Histopathological Analysis. Sci Rep* 2017;7. https://doi.org/10.1038/s41598-017-14786-y.
8. Rezado Y, Jouvion G, Patriarca A, et al. *Proton minibeam radiation therapy widens the therapeutic index for high-grade gliomas. Sci Rep* 2018;8. https://doi.org/10.1038/s41598-018-34796-8.
9. Prezado Y, Martinez-Rovira I, Thengumpallil S, Deman P. *Dosimetry protocol for the preclinical trials in white-beam minibeam radiation therapy. Med Phys* 2011;38:5012-5020.
10. Girst S, Greubel C, Reindl J, et al. Proton minibeam radiation rherapy reduces side effects in an in vivo mouse ear model. *Int J Radiat Oncol Biol Phys* 2016;95:234-241.
11. Zlobinskaya O, Girst S, Greubel C, et al. Reduced side effects by proton microchannel radiotherapy: Study in a human skin model. *Radiat Environ Biophys* 2013;52:123-133.
12. Lamirault C, Doyère V, Juchaux M, et al. *Short and long-term evaluation of the impact of proton minibeam radiation therapy on motor, emotional and cognitive functions. Sci Rep* 2020;10. https://doi.org/10.1038/s41598-020-70371-w.
13. Sotiropoulos M, Brisebard E, Dudal ML, et al. *X-rays minibeam radiation therapy at a conventional irradiator: Pilot evaluation in F98-glioma bearing rats and dose calculations in a human phantom. Clin Transl Radiat Oncol* 2021;27:44-49.
14. Yovino S, Kleinberg L, Grossman SA, Narayanan M, Ford E. The etiology of treatment-related lymphopenia in patients with malignant gliomas: Modeling radiation dose to circulating lymphocytes explains clinical observations and suggests methods of modifying the impact of radiation on immune cells. *Cancer Invest* 2013;31:140-144.
15. Potez M, Fernandez-Palomo C, Bouchet A, et al. Synchrotron microbeam radiation therapy as a new approach for the treatment of radioresistant melanoma: Potential underlying mechanisms. *Int J Radiat Oncol Biol Phys* 2019;105:1126-1136.
16. Johnsrud AJ, Jenkins SV, Jamshidi-Parsian A, et al. Evidence for early stage anti-tumor immunity elicited by spatially fractionated radiotherapy-immunotherapy combinations. *Radiat Res* 2020;194:688-697.
17. Lamirault C, Brisebard E, Patriarca A, et al. *Spatially Modulated Proton Minibeams Results in the Same Increase of Lifespan as a Uniform Target Dose Coverage in F98-Glioma-Bearing Rats. Radiat Res* 2020;194:715-723.
18. Prezado Y, Jouvion G, Guardiola C, et al. *Tumor Control in RG2 Glioma-Bearing Rats: A Comparison Between Proton Minibeam Therapy and Standard Proton Therapy. Int J Radiat Oncol Biol Phys* 2019;104:266-271.

19. Bertho A, Ortiz R, Juchaux M, et al. *First Evaluation of Temporal and Spatial Fractionation in Proton Minibeam Radiation Therapy of Glioma-Bearing Rats. Cancers (Basel)* 2021;13 4865. https://doi.org/10.3390/cancers13194865.
20. Kanagavelu S, Gupta S, Wu X, et al. In vivo effects of lattice radiation therapy on local and distant lung cancer: Potential role of immunomodulation. *Radiat Res* 2014;182:149-162.
21. Fernandez-Palomo C, Schultke E, Smith R, et al. Bystander effects in tumor-free and tumor-bearing rat brains following irradiation by synchrotron x-rays. *Int J Radiat Biol Phys* 2013;89:445-453.
22. Forrester HB, Lobachevsky PN, Stevenson AW, Hall CJ, Martin OA, Sprung CN. Abscopal gene expression in response to synchrotron radiation indicates a role for immunological and DNA damage response genes. *Radiat Res* 2020;194:678-687.
23. Ventura J, Lobachevsky PN, Palazzolo JS, et al. Localized synchrotron irradiation of mouse skin induces persistent systemic genotoxic and immune responses. *Cancer Res* 2017;77:6389-6399.
24. Asur RS, Sharma S, Chang C-W, et al. Spatially fractionated radiation induces cytotoxicity and changes in gene expression in bystander and radiation adjacent murine carcinoma cells. *Radiat Res* 2012;177:751-765.
25. Bouchet A, Serduc R, Laissue JA, Djonov V. Effects of microbeam radiation therapy on normal and tumoral blood vessels. *Phys Med* 2015;31:634-641.
26. Sabatasso S, Laissue JA, Hlushchuk R, et al. Microbeam radiation-induced tissue damage depends on the stage of vascular maturation. *Int J Radiat Oncol Biol Phys* 2011;80:1522-1532.
27. Bouchet A, Sakakini N, El Atifi M, et al. Early gene expression analysis in 9L orthotopic tumor-bearing rats identifies immune modulation in molecular response to synchrotron microbeam radiation therapy. *PLoS One* 2013;8:e81874.
28. Stone HB, Peters LJ, Milas L. Effect of host immune capability on radiocurability and subsequent transplantability of a murine fibrosarcoma. *J Natl Cancer Inst* 1979;63:1229-1235.
29. Vanpouille-Box C, Alard A, Aryankalayil MJ, et al. DNA exonuclease Trex1 regulates radiotherapy-induced tumour immunogenicity. *Nat Commun* 2017;8:15618.
30. Grapin M, Richard C, Limagne E, et al. Optimized fractionated radiotherapy with anti-PD-L1 and anti-TIGIT: A promising new combination. *J Immunother Cancer* 2019;7:160.
31. Herrera FG, Ronet C, Ochoa de Olza M, et al. Low-dose radiotherapy reverses tumor immune desertification and resistance to immunotherapy. *Cancer Discov* 2022;12:108-133.
32. Adam JF, Joubert A, Biston M-C, et al. Prolonged survival of Fischer rats bearing F98 glioma after iodine-enhanced synchrotron stereotactic radiotherapy. *Int J Radiat Oncol Biol Phys* 2006;64:603-611.
33. Barth RF, Kaur B. Rat brain tumor models in experimental neuro-oncology: The C6, 9L, T9, RG2, F98, BT4C, RT-2 and CNS-1 gliomas. *J Neurooncol* 2009;94:299-312.
34. Piotrowski AF, Nirschl TR, Velarde E, et al. Systemic depletion of lymphocytes following focal radiation to the brain in a murine model. *Oncoimmunology* 2018;7:e1445951.
35. Boustani J, Grapin M, Laurent P-A, Apetoh L, Mirjolet C. The 6th R of radiobiology: Reactivation of anti-tumor immune response. *Cancers (Basel)* 2019;11:860.
36. Wang Y. Advances in hypofractionated irradiation-induced immunosuppression of tumor microenvironment. *Front Immunol* 2020;11:612072.
37. De Martino MC, Daviaud C, Vanpouille-Box C. Radiotherapy: An immune response modifier for immuno-oncology. *Semin Immunol* 2021;52:101474.
38. Brown NF, Carter TJ, Ottaviani D, Mulholland P. Harnessing the immune system in glioblastoma. *Br J Cancer* 2018;119:1171-1181.
39. Bazyar S, O'Brien III ET, Benefield T, et al. Immune-mediated effects of microplanar radiotherapy with a small animal irradiator. *Cancers (Basel)* 2021;14:155.
40. Smyth LML, Crosbie JC, Sloggett C, Rogers PAW, Donoghue JF. Spatially fractionated x-ray microbeams elicit a more sustained immune and inflammatory response in the brainstem than homogenous irradiation. *Radiat Res* 2021;196:355-365.
41. Yang Y, Swierczak A, Ibahim M, et al. Synchrotron microbeam radiotherapy evokes a different early tumor immunomodulatory response to conventional radiotherapy in EMT6.5 mammary tumors. *Radiother Oncol* 2019;133:93-99.
42. Hedrich CM, Bream JH. Cell type-specific regulation of IL-10 expression in inflammation and disease. *Immunol Res* 2010;47:185-206.
43. Mocellin S, Marincola F, Rossi CR, Nitti D, Lise M. The multifaceted relationship between IL-10 and adaptive immunity: Putting together the pieces of a puzzle. *Cytokine Growth Factor Rev* 2004;15:61-76.
44. Weber R, Groth C, Lasser S, et al. IL-6 as a major regulator of MDSC activity and possible target for cancer immunotherapy. *Cell Immunol* 2021;359:104254.
45. Lugade AA, Sorenson EW, Gerber SA, et al. Radiation-induced IFN-gamma production within the tumor microenvironment influences antitumor immunity. *J Immunol* 2008;180:3132-3139.
46. Gerber SA, Sedlacek AL, Cron KR, Murphy SP, Frelinger JG, Lord EM. IFN-gamma mediates the antitumor effects of radiation therapy in a murine colon tumor. *Am J Pathol* 2013;182:2345-2354.
47. Page MJ, Bester J, Pretorius E. The inflammatory effects of TNF-alpha and complement component 3 on coagulation. *Sci Rep* 2018;8:1812.
48. Chiang CS, Hong JH, Stalder A, Sun JR, Withers HR, McBride WH. Delayed molecular responses to brain irradiation. *Int J Radiat Biol Oncol Phys* 1997;72:45-53.
49. Wilson CM, Gaber MW, Sabek OM, Zawaski JA, Merchant TE. Radiation-induced astrogliosis and blood-brain barrier damage can be abrogated using anti-TNF treatment. *Int J Radiat Oncol Biol Phys* 2009;74:934-941.
50. Liu Q, Hao Y, Du R, et al. Radiotherapy programs neutrophils to an antitumor phenotype by inducing mesenchymal-epithelial transition. *Transl Lung Cancer Res* 2021;10:1424-1443.
51. Wang L, Jiang J, Chen Y, Jia Q, Chu Q. The roles of CC chemokines in response to radiation. *Radiat Oncol* 2022;17:63.
52. Laumont CM, Banville AC, Gilardi M, Hollern DP, Nelson BH. Tumour-infiltrating B cells: Immunological mechanisms, clinical impact and therapeutic opportunities. *Nat Rev Cancer* 2022;22:414-430.
53. Cabrita R, Lauss M, Sanna A, et al. Tertiary lymphoid structures improve immunotherapy and survival in melanoma. *Nature* 2020;577:561-565.
54. Helmink BA, Reddy SM, Gao J, et al. B cells and tertiary lymphoid structures promote immunotherapy response. *Nature* 2020;577:549-555.
55. Petitprez F, de Reyniès A, Keung EZ, et al. B cells are associated with survival and immunotherapy response in sarcoma. *Nature* 2020;577:556-560.
56. Oh DY, Fong L. Cytotoxic CD4(+) T cells in cancer: Expanding the immune effector toolbox. *Immunity* 2021;54:2701-2711.
57. St Paul M, Ohashi PS. The roles of CD8(+) T cell subsets in antitumor immunity. *Trends Cell Biol* 2020;30:695-704.
58. Zhang Z, Liu S, Zhang B, Qiao L, Zhang Y, Zhang Y. T Cell dysfunction and exhaustion in cancer. *Front Cell Dev Biol* 2020;8:17.
59. Eling L, Bouchet A, Ocadiz A, et al. Unexpected benefits of multiport synchrotron microbeam radiation therapy for brain tumors. *Cancers (Basel)* 2021;13:936.
60. Liao JK. Linking endothelial dysfunction with endothelial cell activation. *J Clin Invest* 2013;123:540-541.
61. Vuillefroy de Silly R, Dietrich PY, Walker PR. Hypoxia and antitumor CD8(+) T cells: An incompatible alliance? *Oncoimmunology* 2016;5:e1232236.
62. Baklaushev VP, Kilpeläinen A, Petkov S, et al. Luciferase expression allows bioluminescence imaging but imposes limitations on the orthotopic mouse (4T1) model of breast cancer. *Sci Rep*. 2017;7:7715.
63. Liao JB, Ovenell KJ, Curtis EEM, et al. Preservation of tumor-host immune interactions with luciferase-tagged imaging in a murine model of ovarian cancer. *J Immunother Cancer* 2015;3:16.
64. Ceberg C, Jönsson B-A, Prezado Y, et al. Photon activation therapy of RG2 glioma carrying Fischer rats using stable thallium and monochromatic synchrotron radiation. *Phys Med Biol* 2012;57:8377-8391.

ARTICLE IN PRESS

65. Aas AT, Brun A, Blennow C, Strömblad S, Salford LG. The RG2 rat glioma model. *J Neurooncol* 1995;23:175-183.
66. Colton M, Cheadle EJ, Honeychurch J, Illidge TM. Reprogramming the tumour microenvironment by radiotherapy: Implications for radiotherapy and immunotherapy combinations. *Radiat Oncol* 2020;15:254.
67. Demaria S, Guha C, Schoenfeld J, et al. Radiation dose and fraction in immunotherapy: One-size regimen does not fit all settings, so how does one choose? *J Immunother Cancer* 2021;9: e002038.
68. Ngwa W, Irabor OC, Schoenfeld JD, Hesser J, Demaria S, Formenti SC. Using immunotherapy to boost the abscopal effect. *Nat Rev Cancer* 2018;18:313-322.
69. Mohiuddin M, Fujita M, Regine WF, Megooni AS, Ibbott GS, Ahmed MM. High-dose spatially-fractionated radiation (GRID): A new paradigm in the management of advanced cancers. *Int J Radiat Oncol Biol Phys* 1999;45:721-727.
70. Amendola BE, Perez NC, Wu X, Amendola MA, Qureshi IZ. Safety and efficacy of lattice radiotherapy in voluminous non-small cell lung cancer. *Cureus* 2019;11:e4263.